Journal of Applied Physics

RESEARCH ARTICLE | OCTOBER 22 2025

Electronic transport properties and stability of 2D electron gases on $Si_3N_4/AlO_x//KTaO_3$ heterostructures

R. S. Silva, Jr. ; A. M. Merodio ; E. A. Martínez ; F. Gallego ; N. M. Nemes ; F. Y. Bruno

J. Appl. Phys. 138, 165301 (2025)
https://doi.org/10.1063/5.0293470

AIP Publishing

Journal of Applied Physics ARTICLE pubs.aip.org/aip/jap

Electronic transport properties and stability of 2D electron gases on $Si_3N_4/AlO_x//KTaO_3$ heterostructures

Cite as: J. Appl. Phys. **138**, 165301 (2025); doi: 10.1063/5.0293470
Submitted: 28 July 2025 · Accepted: 6 October 2025 ·
Published Online: 22 October 2025

View Online Export Citation CrossMark

R. S. Silva, Jr.,[1] A. M. Merodio,[1] E. A. Martínez,[2] F. Gallego,[1] N. M. Nemes,[1] and F. Y. Bruno[1,a)]

AFFILIATIONS

[1]GFMC, Departamento de Física de Materiales, Universidad Complutense de Madrid, Madrid E-28040, Spain
[2]Dipartimento di Scienze Fisiche e Chimiche, Università degli Studi dell'Aquila, L'Aquila 67100, Italy

[a)]**Author to whom correspondence should be addressed:** fybruno@ucm.es

ABSTRACT

We report on the successful stabilization of a two-dimensional electron gas (2DEG) in $Si_3N_4/AlO_x//KTaO_3(001)$ heterostructures. Electronic transport measurements reveal that the AlO_x layer thickness critically modulates the 2DEG mobility, with an optimal thickness achieving a mobility of $\mu \approx 444\ cm^2\ V^{-1}\ s^{-1}$ at 10 K, which is, despite the amorphous granular nature of the AlO_x layers, comparable to epitaxial oxide-based 2DEGs. Thicker AlO_x layers reduce mobility and induce a Kondo-like upturn in resistance at low temperatures, which is attributed to oxygen depletion extending into the substrate and enhancing defect scattering. Additionally, the samples remain metallic after six months of exposure to ambient conditions, with high-mobility samples maintaining stable carrier densities and mobilities and experiencing only minor increases in sheet resistance over time. These findings highlight the potential of $KTaO_3$ 2DEGs for long-term electronic applications, providing valuable insights for optimizing oxide heterostructures for future device technologies.

I. INTRODUCTION

Transition metal oxides (TMOs) display a remarkable variety of electronic phases, driven by the strong interplay among their lattice, charge, spin, and orbital degrees of freedom. A breakthrough in this field was the 2004 discovery of a high-mobility two-dimensional electron gas (2DEG) at the interface between the band insulators, $LaAlO_3$ (LAO) and $SrTiO_3$ (STO), which initiated intense research into 2D oxide-based electronic systems.[1,2] While STO-based 2DEGs remain the most widely studied, $KTaO_3$ (KTO)-based heterostructures have recently attracted significant attention due to their distinct properties.[3] KTO is a wide gap (3.5 eV) band insulator with a cubic perovskite structure and a strong spin–orbit coupling strength of approximately 0.4 eV arising from its heavy Ta 5*d* electrons.[4,5] Additionally, KTO is an incipient quantum ferroelectric that becomes metallic when lightly doped with oxygen vacancies or via chemical substitution.[4,6,7] These characteristics make KTO an excellent platform for stabilizing two-dimensional electron systems with potentially unique electronic and spintronic functionalities.

Multiple approaches have been employed to stabilize 2DEGs in KTO, including the growth of epitaxial oxide layers such as $LaTiO_3$ and EuO, the deposition of amorphous oxides like $LaAlO_3$ and $CaZrO_3$, and ionic liquid gating.[8–12] The versatility of these methods has enabled the discovery of diverse and tunable properties in KTO-based 2DEGs.[10,13–16] Among these strategies, the direct deposition of thin amorphous Al layers on KTO offers a simple and effective route. In this process, a redox reaction at the Al/KTO interface oxidizes the Al into AlO_x by extracting oxygen from the KTO substrate, thereby creating oxygen vacancies (V_Os) near the surface.[13,17,18] These vacancies act as electron donors, inducing a 2DEG at the interface. The spatial distribution of V_Os critically influences carrier density and mobility, while disorder and defect scattering play key roles in phenomena such as superconductivity in these systems.[19–22] However, such vacancy-stabilized 2DEGs may be metastable, as oxygen vacancies can be annihilated over time through atmospheric oxygen diffusion.[23] Although Si_3N_4 has been demonstrated to act as an effective barrier against oxygen diffusion, the long-term stability of these heterostructures remains largely unexplored.[21]

In this work, we fabricate Si_3N_4/AlO_x//KTO(001) heterostructures via magnetron sputter deposition to stabilize robust 2DEGs. We systematically investigate their electronic transport properties and demonstrate that the AlO_x thickness is a key parameter controlling mobility, with low-temperature values reaching $\mu \approx 444\ cm^2\ V^{-1}\ s^{-1}$, comparable to those of epitaxially grown oxide interfaces. Furthermore, we evaluate the temporal stability of these heterostructures over a six-month period, demonstrating that high-mobility samples retain stable carrier densities and mobilities, with only marginal increases in sheet resistance (R_S). These results underscore the potential of Al-induced KTO 2DEGs for long-term electronic applications and offer valuable insights for optimizing oxide heterostructures for future device technologies.

II. METHODS

The Si_3N_4/AlO_x//KTO heterostructures were fabricated by growing amorphous Al and Si_3N_4 layers on KTO(001) single crystals using magnetron sputtering. Prior to deposition, the KTO substrates were annealed *in situ* at 500 °C for 40 min under a pressure below 10^{-7} mbar to ensure surface cleanliness.[24] The amorphous Al layer was then deposited by DC magnetron sputtering under an Ar atmosphere of 7.4×10^{-3} mbar at a temperature of 250 °C following the procedure described in Ref. 21. Subsequently, the Si_3N_4 passivation layer was deposited by RF magnetron sputtering at the same Ar pressure. The Al layer both oxidizes into AlO_x and generates V_Os within the KTO substrate, resulting in a conducting 2DEG at the AlO_x//KTO interface.[21] The samples grown with different thicknesses are summarized in Table I, and a schematic of the heterostructure is shown in Fig. 1(a). After removing the samples from the growth chamber, they were mounted on measurement pucks, and electrical contacts were fabricated by Al-wire ultrasonic bonding in a van der Pauw configuration.[25] The samples remained mounted for the six-month duration of the experiment to avoid differences arising from repeated contact fabrication. Magneto-transport measurements were performed using a Physical Property Measurement System (PPMS) from Quantum Design, allowing temperature control down to 2 K and magnetic fields ranging from −5 to +5 T. The PPMS system was equipped with an external switch box that enabled current injection and voltage measurement in different contact configurations of the square samples. The sheet resistance R_S was obtained by the van der Pauw method.[26] Monitoring of the room-temperature resistance measurements over the six-month period was performed using a four-tip probe station equipped with a Keithley 2450 Source Measure Unit (SMU) from Tektronix.

TABLE I. Summary of the Si_3N_4/AlO_x//$KTaO_3$ heterostructures used in this work, indicating the thicknesses of the AlO_x and Si_3N_4 layers.

Heterostructure no.	AlO_x thickness (nm)	Si_3N_4 thickness (nm)
1	2.9	5
2	3.2	5
3	3.5	5
4	4.5	5
5	7.5	5

III. RESULTS AND DISCUSSION

A. Electronic transport properties

Figure 1(b) shows the temperature-dependent sheet resistance $R_S(T)$ for Si_3N_4/AlO_x//KTO(001) heterostructures with varying AlO_x layer thicknesses, as summarized in Table I. All heterostructures exhibit metallic behavior ($dR_S/dT > 0$), as R_S decreases monotonically with decreasing temperature from 300 to 30 K, consistent with the presence of an interfacial 2DEG.[10,21] The room-temperature R_S varies with the AlO_x layer thickness, increasing from 1.2×10^4 to $1 \times 10^5\ \Omega\ sq^{-1}$, although this dependence is not monotonic.

At temperatures below 30 K, an R_S upturn reminiscent of the Kondo effect is observed,[27] particularly in heterostructures with thicker AlO_x layers (#3, #4, and #5). In contrast, samples with thinner AlO_x layers (#1 and #2) exhibit a much subtler upturn. The Kondo effect in 2DEGs arises from the scattering of conduction

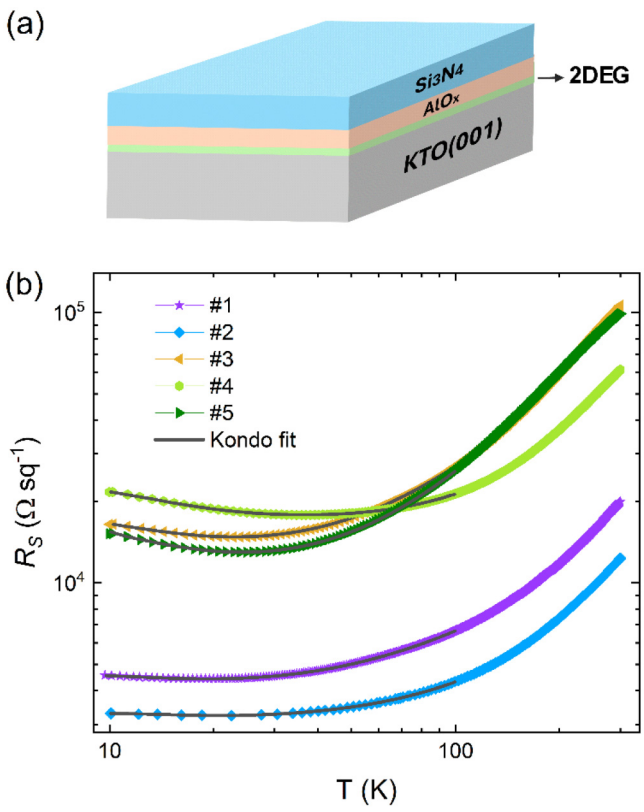

FIG. 1. (a) Schematic of the heterostructures in the present study. (b) Temperature-dependent sheet resistance (R_S) for the Si_3N_4/AlO_x//KTO(001) heterostructures with different AlO_x thicknesses. The black solid line shows the Kondo fit below 100 K of $R_S(T)$ for the samples #3, #4, and #5 using Eq. (1).

TABLE II. Parameters obtained using Eq. (1) by fitting $R_S(T)$ data below 100 K compared with values obtained from the indicated references in similar heterostructures.

Heterostructure no.	R_0 (Ω sq^{-1})	a (Ω sq^{-1} K^q)	q	C (Ω sq^{-1})	T_K (K)	S
1	3 341 ± 79	16.2 ± 1.7	1.15 ± 0.02	746 ± 63	14.8 ± 0.2	0.14 ± 0.02
2	3 049 ± 13	0.7 ± 0.07	1.6 ± 0.02	137 ± 11	15.8 ± 0.3	0.04 ± 0.01
3	10 382 ± 220	21.89 ± 1.44	1.43 ± 0.01	4711 ± 320	12.3 ± 0.4	0.12 ± 0.01
4	16 020 ± 70	0.73 ± 0.08	1.92 ± 0.02	4561 ± 140	12.6 ± 0.2	0.08 ± 0.01
5	8 337 ± 240	13.71 ± 0.88	1.54 ± 0.01	6084 ± 500	10.9 ± 0.5	0.14 ± 0.01
$LaAlO_3$/KTO[27]	2 723.8	2.16	2.04	2509	15.6	0.12
$CaZrO_3$/KTO[29]	…	…	…	…	20.2	0.13

electrons by localized magnetic moments (e.g., from impurities or V_Os) leading to characteristic low-temperature R_S upturn. The temperature dependence of this magnetic impurity contribution to resistance follows a universal function characterized by a single temperature scale, the Kondo temperature (T_K).[28] We fitted the $R_S(T)$ data below 100 K using the following equation:[29]

$$R_S = R_0 + aT^q + C\left[\frac{\ln(T/T_K)}{\sqrt{(\ln(T/T_K))^2 + \pi^2 S(S+1)}}\right], \quad (1)$$

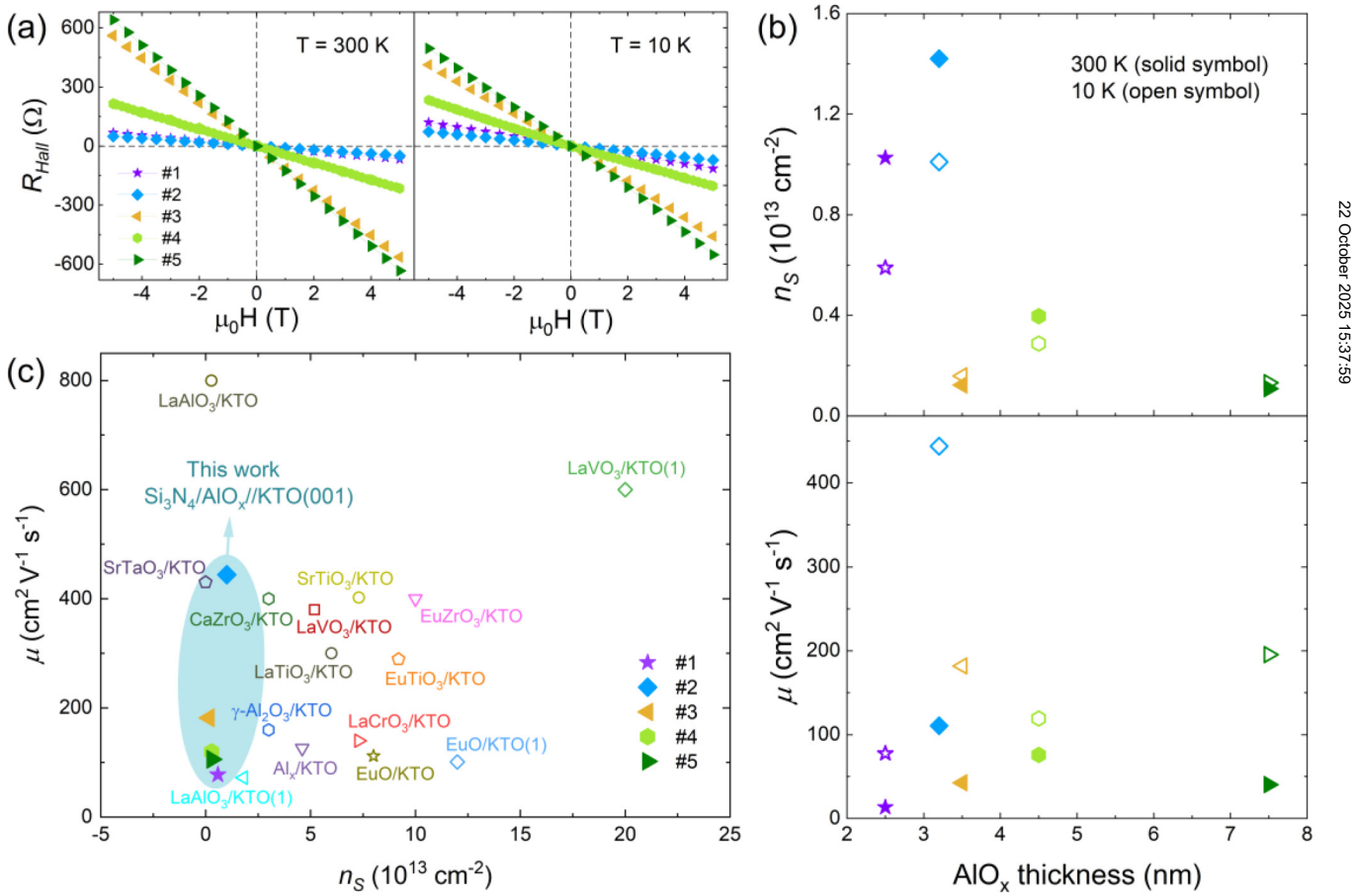

FIG. 2. (a) Hall resistance (R_{Hall}) measured for all heterostructures at 300 and 10 K. (b) Sheet carrier density n_s and mobility μ as a function of the AlO_x thickness on the Si_3N_4/AlO_x//$KTaO_3$ heterostructures. (c) Comparative overview of sheet carrier densities and mobilities at low temperature ($T \leq 10$ K) of all heterostructures with various typical KTO-based heterostructures from references.[8,14,21,27,29,31–37]

where R_0 is the residual resistance due to sample disorder, aT^q describes the transport behavior determined by electron–electron and electron–phonon interactions, and S is the effective spin of the magnetic scattering centers.[29] As observed by the black solid line fits shown in Fig. 1(b), the data for samples #3, #4, and #5 can be well described by Eq. (1). We note that weak localization and weak antilocalization may also contribute to low-temperature transport in KTO-based 2DEGs, as reported in related systems, although these effects are most prominent below ~3 K and are unlikely to dominate in our 10–300 K measurements.[30] Table II summarizes the obtained values of the fitted parameters. These values are comparable with those previously reported for other KTO-based 2DEGs such as $LaAlO_3/KTaO_3$[27] and $CaZrO_3/KTaO_3$.[29] The origin of this effect is rationalized by the scattering on the Ta^{4+} ions induced by the presence of oxygen vacancies in the substrate.[27,31] The values obtained for T_K fall within the 10–16 K range for all samples, suggesting a common origin for the R_S upturn. However, heterostructures #1 and #2 exhibit values of the parameter C, which effectively weights the Kondo upturn, that is an order of magnitude lower.

To gain further insight into the electronic transport properties of the samples, we evaluated the Hall resistance (R_{Hall}), sheet carrier density (n_s), and mobility (μ). Figure 2(a) shows the magnetic field dependence of R_{Hall} measured for all heterostructures at 300 and 10 K, respectively. The linear behavior and negative slopes observed at both temperatures indicate that electrons are the primary carriers and that conduction is dominated by a single band.[31] From R_{Hall} curves, we calculate the sheet carrier density and mobility, respectively, through $n_S = B/q|R_{Hall}|$ and $\mu = 1/qn_SR_S$, where B is the magnetic field and q is the unit charge.

Figure 2(b) shows n_s and μ at 300 K (solid symbols) and 10 K (open symbols), respectively, as a function of AlO_x thickness. The carrier density exhibits a slight increase, whereas the mobility shows a pronounced decrease with increasing temperature.[27,29,32] A comparison of low temperature n_s and μ values from this study with data reported in other works is shown in Fig. 2(c). The variations observed cannot be solely attributed to the growth technique or to the interfacing material, other factors such as growth conditions and substrate surface treatment likely play a role. In the following, we discuss the transport characteristics of our samples.

Starting from an insulating KTO substrate, charge carriers are introduced via V_Os formed through the efficient redox reaction at the Al//KTO interface. The distribution of V_Os within the substrate depends on the thickness of the deposited Al layer. The thicker the Al layers, the more extended the regions of V_Os and reduced Ta^{4+} ions effectively setting a lower bound for the thickness of the 2DEG. In KTO(110), we previously measured the oxygen depletion depth to be in the 3–5 nm range depending on AlO_x thickness,[21] comparable values of ~4 nm have been reported for the conducting region in KTO(111) interfaces, tunable between 2 and 6 nm under gate voltage.[22] These observations suggest that in our system the conducting layer is confined within only a few nanometers of the interface and overlaps with the defect-rich areas that act as scattering centers.[21] Sample #2 achieves a low-temperature mobility of $\mu \approx 444\ cm^2\ V^{-1}\ s^{-1}$ at 10 K, exceeding the values obtained at some epitaxial interfaces such as γ-Al_2O_3/KTO,[14] $LaCrO_3/KTO$,[36] and EuO/KTO.[32] Its low-temperature R_S is nearly temperature-independent; however, deviating from this optimal AlO_x thickness results in decreased mobility. We interpret this result as a consequence of the extended V_Os' defects region related to the thicker AlO_x layers. The observation of a more noticeable Kondo-like upturn in samples with thicker AlO_x layers support this interpretation as this enhanced effect may arise from the scattering with magnetic Ta^{4+} ions or V_Os. The samples in this study exhibit relatively low carrier densities of $n_s \approx 1.0 \times 10^{13}\ cm^{-2}$, as indicated by the shaded blue region of Fig. 2(c). By contrast, most high density 2DEGs are obtained via epitaxial oxide growth on KTO. We propose that the granular and amorphous nature of the AlO_x layer in our heterostructures results in a non-uniform 2DEG or is less effective in creating V_Os due to spatial inhomogeneity, thereby limiting the achievable carrier density.

B. Temporal stability of electronic transport properties

Following the temperature-dependent electronic transport characterization, we maintained the heterostructures mounted on the measurement pucks to monitor their evolution over six months. Figure 3 shows the room-temperature (RT) R_s measurements taken with a tabletop four-point probe station at the following time intervals: 1 day, 10 days, 1 month, 3 months, and 6 months. During this period, the samples were stored under ambient conditions and remained exposed to the atmosphere. Then, to further demonstrate the stability of the heterostructures after 180 days, we repeated the temperature-dependent resistance and Hall resistance measurements (at 10 and 300 K), enabling the calculation of sheet resistance, sheet carrier density, and mobility, as shown in Fig. 4.

The RT–R_s increases over time for all samples as shown in Fig. 3. In particular, sample #2 with optimal low temperature mobility presents a variation of RT–R_S from day 1 to day 180 of $R_S^{1}/R_S^{180} = 0.9$, whereas #4 presents ratios of $R_S^{1}/R_S^{180} = 0.2$. This

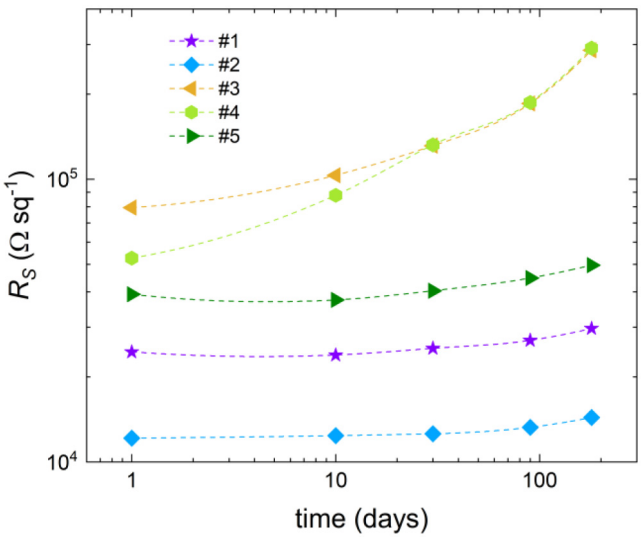

FIG. 3. Room-temperature sheet resistance evolution with time.

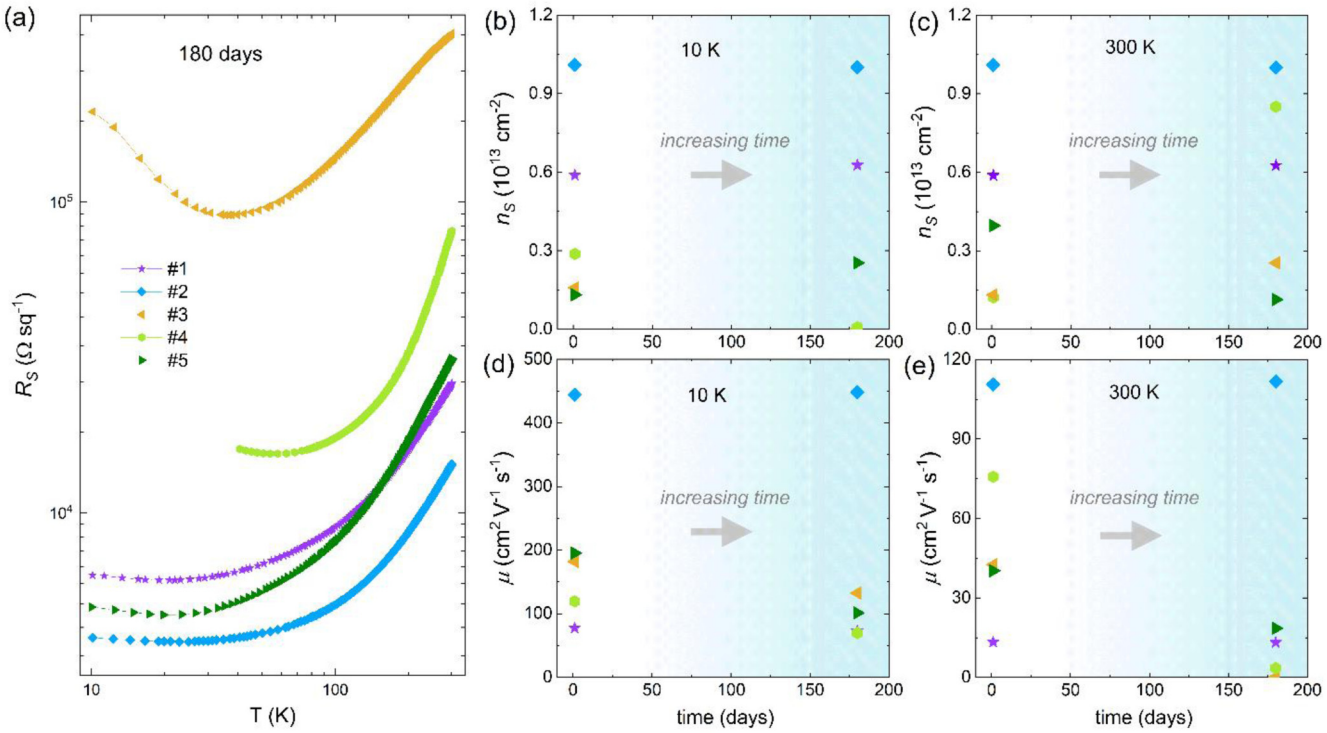

FIG. 4. (a) Temperature-dependent sheet resistance (R_S) for the Si_3N_4/AlO_x//$KTaO_3$(001) heterostructures with different AlO_x thicknesses. (b) and (c) Sheet carrier density (n_s) and (d) and (e) mobility (μ) at 10 and 300 K, respectively, for the heterostructures.

demonstrated that sample #2 with high optimal mobility is more stable over time. The heterostructures that exhibit the largest increase in R_S with time (#3, #4, and #5) also exhibited the most pronounced Kondo upturn on the electronic transport properties, which are the ones with thicker AlO_x layers. The increase in R_s and changes in mobility and carrier density can be explained by oxygen ion diffusion from the atmosphere, V_Os clustering in KTO, among other effects.[23,27] Lastly, it is important to highlight the temporal and thermal stability of sample #2, with carrier density and mobility varying by less than 5% between 10 and 300 K over 180 days.

IV. CONCLUSIONS

In summary, we successfully stabilized a two-dimensional electron gas (2DEG) in Si_3N_4/AlO_x//$KTaO_3$(001) heterostructures. Systematic electronic transport characterization revealed that the AlO_x layer thickness is a critical parameter for tuning the 2DEG properties. An optimal thickness yielded a 10 K mobility of $\mu \approx 444$ cm^2 V^{-1} s^{-1}, comparable to values reported for 2DEGs in KTO-based epitaxial oxide interfaces, despite the amorphous and granular nature of our AlO_x layers. Samples with thicker AlO_x layers exhibited reduced mobility and an upturn in low-temperature resistance, reminiscent of the Kondo effect. We attribute this behavior to the deeper extension of the oxygen depletion region into the substrate, which overlaps with the 2DEG and enhances defect scattering. Finally, long-term stability measurements of the electronic properties over 180 days showed that high-mobility samples maintained stable carrier densities and mobilities, with only a marginal increase in R_s during this timeframe, demonstrating their suitability for experiments lasting at least several months.

ACKNOWLEDGMENTS

This work has been supported by Comunidad de Madrid (Atraccion de Talento Grant No. 2022-5A/IND-24230), Grant Nos. CNS2022-135485 and TED2021-129254B-C21 funded by MCIN/AEI/10.13039/501100011033 and European Union NextGeneration EU/PRTR. E.A.M. acknowledges financial support under the National Recovery and Resilience Plan (NRRP), Mission 4, Component 2, Investment 1.1, funded by the European Union NextGenerationEU—Project Title "Symmetry-broken HEterostructurEs for Photovoltaic applications-SHEEP"—CUP B53D23028580001—Grant Assignment Decree No. 1409 adopted on 14 September 2022 by the Italian Ministry of University and Research (MUR). The authors acknowledge Professor Jacobo Santamaría for providing laboratory facilities and institutional support.

AUTHOR DECLARATIONS

Conflict of Interest

The authors have no conflicts to disclose.

Author Contributions

R. S. Silva Jr.: Conceptualization (equal); Formal analysis (lead); Investigation (lead); Project administration (supporting); Visualization (lead); Writing – original draft (lead); Writing – review & editing (supporting). **A. M. Merodio:** Investigation (supporting); Methodology (supporting). **E. A. Martínez:** Investigation (supporting); Methodology (supporting); Writing – review & editing (supporting). **F. Gallego:** Investigation (supporting); Methodology (supporting); Writing – review & editing (supporting). **N. M. Nemes:** Investigation (supporting); Project administration (supporting); Resources (supporting); Supervision (supporting); Writing – review & editing (supporting). **F. Y. Bruno:** Conceptualization (equal); Formal analysis (equal); Funding acquisition (equal); Methodology (equal); Supervision (equal); Writing – review & editing (equal).

DATA AVAILABILITY

The data that support the findings of this study are available from the corresponding author upon reasonable request.

REFERENCES

[1]A. Ohtomo and H. Y. Hwang, "A high-mobility electron gas at the $LaAlO_3$/$SrTiO_3$ heterointerface," Nature **427**(6973), 423 (2004).

[2]M. Coll, J. Fontcuberta, M. Althammer, M. Bibes, H. Boschker, A. Calleja, G. Cheng, M. Cuoco, R. Dittmann, B. Dkhil, I. E. Baggari, M. Fanciulli, I. Fina, E. Fortunato, C. Frontera, S. Fujita, V. Garcia, S. T. B. Goennenwein, C. G. Granqvist, J. Grollier, R. Gross, A. Hagfeldt, G. Herranz, K. Hono, E. Houwman, M. Huijben, A. Kalaboukhov, D. J. Keeble, G. Koster, L. F. Kourkoutis, J. Levy, M. Lira-Cantu, J. L. MacManus-Driscoll, J. Mannhart, R. Martins, S. Menzel, T. Mikolajick, M. Napari, M. D. Nguyen, G. Niklasson, C. Paillard, S. Panigrahi, G. Rijnders, F. Sánchez, P. Sanchis, S. Sanna, D. G. Schlom, U. Schroeder, K. M. Shen, A. Siemon, M. Spreitzer, H. Sukegawa, R. Tamayo, J. van den Brink, N. Pryds, and F. M. Granozio, "Towards oxide electronics: A roadmap," Appl. Surf. Sci. **482**, 1–93 (2019).

[3]A. Gupta, H. Silotia, A. Kumari, M. Dumen, S. Goyal, R. Tomar, N. Wadehra, P. Ayyub, and S. Chakraverty, "$KTaO_3$—The new kid on the spintronics block," Adv. Mater. **34**(9), 2106481 (2022).

[4]S. H. Wemple, "Some transport properties of oxygen-deficient single-crystal potassium tantalate ($KTaO_3$)," Phys. Rev. **137**(5A), A1575 (1965).

[5]F. Y. Bruno, S. McKeown Walker, S. Riccò, A. de la Torre, Z. Wang, A. Tamai, T. K. Kim, M. Hoesch, M. S. Bahramy, and F. Baumberger, "Band structure and spin-orbital texture of the (111)-$KTaO_3$ 2D electron gas," Adv. Electron. Mater. **5**(5), 1800860 (2019).

[6]J. K. Hulm, B. T. Matthias, and E. A. Long, "A ferromagnetic curie point in $KTaO_3$ at very low temperatures," Phys. Rev. **79**(5), 885 (1950).

[7]S. K. Ojha, S. K. Gogoi, P. Mandal, S. D. Kaushik, J. W. Freeland, M. Jain, and S. Middey, "Oxygen vacancy induced electronic structure modification of $KTaO_3$," Phys. Rev. B **103**(8), 085120 (2021).

[8]K. Zou, S. Ismail-Beigi, K. Kisslinger, X. Shen, D. Su, F. J. Walker, and C. H. Ahn, "$LaTiO_3$/$KTaO_3$ interfaces: A new two-dimensional electron gas system," APL Mater. **3**(3), 036104 (2015).

[9]Z. Chen, Z. Liu, Y. Sun, X. Chen, Y. Liu, H. Zhang, H. Li, M. Zhang, S. Hong, T. Ren, C. Zhang, H. Tian, Y. Zhou, J. Sun, and Y. Xie, "Two-dimensional superconductivity at the $LaAlO_3$/$KTaO_3$ (110) heterointerface," Phys. Rev. Lett. **126**(2), 026802 (2021).

[10]C. Liu, X. Yan, D. Jin, Y. Ma, H. W. Hsiao, Y. Lin, T. M. Bretz-Sullivan, X. Zhou, J. Pearson, B. Fisher, J. S. Jiang, W. Han, J. M. Zuo, J. Wen, D. D. Fong, J. Sun, H. Zhou, and A. Bhattacharya, "Two-dimensional superconductivity and anisotropic transport at $KTaO_3$ (111) interfaces," Science **371**(6530), 716 (2021).

[11]H. Zhang, Y. Xiao, Q. Gao, N. Wu, S. Zhou, Y. Wang, M. Wang, D. Tian, L. Chen, W. Qi, D. Zheng, J. Zhang, F. Han, H. Yang, B. Liu, Y. Chen, F. Hu, B. Shen, J. Sun, W. Zhao, and J. Zhang, "Magnetotransport evidence for the coexistence of two-dimensional superconductivity and ferromagnetism at (111)-oriented a-$CaZrO_3$/$KTaO_3$ interfaces," Nat. Commun. **16**(1), 3035 (2025).

[12]K. Ueno, S. Nakamura, H. Shimotani, H. T. Yuan, N. Kimura, T. Nojima, H. Aoki, Y. Iwasa, and M. Kawasaki, "Discovery of superconductivity in $KTaO_3$ by electrostatic carrier doping," Nat. Nanotechnol. **6**(7), 408 (2011).

[13]L. M. Vicente-Arche, J. Bréhin, S. Varotto, M. Cosset-Cheneau, S. Mallik, R. Salazar, P. Noël, D. C. Vaz, F. Trier, S. Bhattacharya, A. Sander, P. Le Fèvre, F. Bertran, G. Saiz, G. Ménard, N. Bergeal, A. Barthélémy, H. Li, C. C. Lin, D. E. Nikonov, I. A. Young, J. E. Rault, L. Vila, J. P. Attané, and M. Bibes, "Spin-charge interconversion in $KTaO_3$ 2D electron gases," Adv. Mater. **33**(43), 2102102 (2021).

[14]S. Qi, H. Zhang, J. Zhang, Y. Gan, X. Chen, B. Shen, Y. Chen, Y. Chen, and J. Sun, "Large optical tunability of 5d 2D electron gas at the spinel/perovskite γ-Al_2O_3/$KTaO_3$ heterointerface," Adv. Mater. Interfaces **9**(20), 2200103 (2022).

[15]E. G. Arnault, A. H. Al-Tawhid, S. Salmani-Rezaie, D. A. Muller, D. P. Kumah, M. S. Bahramy, G. Finkelstein, and K. Ahadi, "Anisotropic superconductivity at $KTaO_3$ (111) interfaces," Sci. Adv. **9**(7), eadf1414 (2023).

[16]H. Zhang, X. Yan, X. Zhang, S. Wang, C. Xiong, H. Zhang, S. Qi, J. Zhang, F. Han, N. Wu, B. Liu, Y. Chen, B. Shen, and J. Sun, "Unusual electric and optical tuning of $KTaO_3$-based two-dimensional electron gases with 5d orbitals," ACS Nano **13**(1), 609 (2019).

[17]T. C. Rödel, F. Fortuna, S. Sengupta, E. Frantzeskakis, P. Le Fèvre, F. Bertran, B. Mercey, S. Matzen, G. Agnus, T. Maroutian, P. Lecoeur, and A. F. Santander-Syro, "Universal fabrication of 2D electron systems in functional oxides," Adv. Mater. **28**(10), 1976 (2016).

[18]E. A. Martínez, J. Dai, M. Tallarida, N. M. Nemes, and F. Y. Bruno, "Anisotropic electronic structure of the 2D electron gas at the AlO_x/$KTaO_3$(110) interface," Adv. Electron. Mater. **9**(10), 2300267 (2023).

[19]F. Gunkel, D. V. Christensen, Y. Z. Chen, and N. Pryds, "Oxygen vacancies: The (in)visible friend of oxide electronics," Appl. Phys. Lett. **116**(12), 120505 (2020).

[20]S. Lee, J. Jeon, and H. Lee, "Probing oxygen vacancy distribution in oxide heterostructures by deep learning-based spectral analysis of current noise," Appl. Surf. Sci. **604**, 154599 (2022).

[21]E. A. Martínez, A. M. Lucero, E. D. Cantero, N. Biškup, A. Orte, E. A. Sánchez, M. Romera, N. M. Nemes, J. L. Martínez, M. Varela, O. Grizzi, and F. Y. Bruno, "Synthesis and in-depth interfacial characterization of 2D electron gases formed in Si_3N_4/Al//$KTaO_3$ heterostructures," Appl. Surf. Sci. **689**, 162499 (2025).

[22]Z. Chen, Y. Liu, H. Zhang, Z. Liu, H. Tian, Y. Sun, M. Zhang, Y. Zhou, J. Sun, and Y. Xie, "Electric field control of superconductivity at the $LaAlO_3$/$KTaO_3$(111) interface," Science **372**(6543), 721 (2021).

[23]G. Huang, P. Zhou, L. Yin, Z. Zhou, S. Gong, R. Zhao, G. Liu, J. Zhang, Y. Li, Y. Jiang, and J. Gao, "Time-dependent resistance of quasi-two-dimensional electron gas on $KTaO_3$," Appl. Phys. Lett. **117**(17), 171603 (2020).

[24]A. M. Lucero Manzano, E. D. Cantero, E. A. Martínez, F. Y. Bruno, E. A. Sánchez, and O. Grizzi, "$KTaO_3$ (001) preparation methods in vacuum: Effects on surface stoichiometry, crystallography and in-gap states," J. Vac. Sci. Technol. B **43**, 044001 (2025).

[25]A. A. Ramadan, R. D. Gould, and A. Ashour, "On the Van der Pauw method of resistivity measurements," Thin Solid Films **239**(2), 272 (1994).

[26]L. J. Van der PAUW, "A method of measuring specific resistivity and Hall effect of discs of arbitrary shape," Philips Res. Rep. **13**, 1 (1958).

[27]H. Zhang, H. Zhang, X. Yan, X. Zhang, Q. Zhang, J. Zhang, F. Han, L. Gu, B. Liu, Y. Chen, B. Shen, and J. Sun, "Highly mobile two-dimensional electron

gases with a strong gating effect at the amorphous $LaAlO_3/KTaO_3$ interface," ACS Appl. Mater. Interfaces **9**(41), 36456 (2017).
[28]M. Lee, J. R. Williams, S. Zhang, C. D. Frisbie, and D. Goldhaber-Gordon, "Electrolyte gate-controlled kondo effect in $SrTiO_3$," Phys. Rev. Lett. **107**(25), 256601 (2011).
[29]S. Qi, J. Liang, G. Shi, Y. Gan, Y. Chen, Y. Chen, and J. Sun, "Creation of two-dimensional electron gas at the heterointerface of $CaZrO_3/KTaO_3$ with tunable Rashba spin-orbit coupling," ACS Appl. Electron. Mater. **6**, 8404 (2024).
[30]Y. Zou, H. Shin, H. Wei, Y. Fan, B. A. Davidson, E. J. Guo, Q. Chen, K. Zou, and Z. G. Cheng, "Transport behaviors of topological band conduction in $KTaO_3$'s two-dimensional electron gases," npj Quantum Mater. **7**(1), 122 (2022).
[31]Z. Fan, Q. Sui, F. Ran, H. Ling, D. Li, Z. Wang, P. Chen, Y. Liang, and J. Zhang, "The origin of magnetic ordering and reduced mobility in $KTaO_3$-based 2DEGs: Interfacial interdiffusion," APL Mater. **12**(7), 071102 (2024).
[32]H. Zhang, Y. Yun, X. Zhang, H. Zhang, Y. Ma, X. Yan, F. Wang, G. Li, R. Li, T. Khan, Y. Chen, W. Liu, F. Hu, B. Liu, B. Shen, W. Han, and J. Sun, "High-mobility spin-polarized two-dimensional electron gases at $EuO/KTaO_3$ interfaces," Phys. Rev. Lett. **121**(11), 116803 (2018).
[33]H. Xu, Y. Gan, Y. Zhao, M. Li, X. Hu, X. Chen, R. Wang, Y. Li, J. Sun, F. Hu, Y. Chen, and B. Shen, "Two-dimensional electron gases at the amorphous and crystalline $SrTiO_3/KTaO_3$ heterointerfaces," Phys. Status Solidi A **220**(13), 2300235 (2023).
[34]N. Wadehra, R. Tomar, R. M. Varma, R. K. Gopal, Y. Singh, S. Dattagupta, and S. Chakraverty, "Planar Hall effect and anisotropic magnetoresistance in polar-polar interface of $LaVO_3$-$KTaO_3$ with strong spin-orbit coupling," Nat. Commun. **11**(1), 874 (2020).
[35]X. Wei, S. Wang, J. Lv, H. Zhu, H. Yan, and K. Jin, "Characterization of the $EuZrO_3/KTaO_3$ interface: Tunable carrier density and long-range spin transport," ACS Appl. Nano Mater. **8**(4), 2006 (2025).
[36]A. H. Al-Tawhid, D. P. Kumah, and K. Ahadi, "Two-dimensional electron systems and interfacial coupling in $LaCrO_3/KTaO_3$heterostructures," Appl. Phys. Lett. **118**(19), 192905 (2021).
[37]X. Zhang, Z. Pang, C. Yin, M. Yan, Y. Y. Lv, Y. Deng, and S. T. Zhang, "Quasi-two-dimensional electron gas and weak antilocalization at the interface of $SrTaO_3/KTaO_3$ heterostructures," Phys. Rev. B **108**(23), 235114 (2023).